10.4 THEORETICAL STUDY OF SCENE IDENTIFICATION AND INVERSION OF SATELLITE-MEASURED RADIANCE TO FLUX

Lin H. Chambers*
NASA Langley Research Center, Hampton, VA

1. INTRODUCTION

An extensive study has been undertaken to theoretically simulate the process space-based instruments require when attempting to determine the flux of radiative energy from a measurement of radiance at a given view angle. This study attempts to model the whole process starting with realistic cloud fields generated from Landsat data. Radiance fields are then computed allowing for horizontal transport using the two-dimensional (2D) radiative transport solver, Spherical Harmonics Discrete Ordinates Method (SHDOM). The computed radiances are then processed the same way the actual measured radiances are processed to produce fluxes. The objective is to understand and quantify the error sources in this entire process. In this paper, algorithms used for the Clouds and the Earth's Radiant Energy System (CERES) instrument on the Tropical Rainfall Measuring Mission (TRMM) and Terra spacecraft are specifically assessed.

2. APPROACH

2.1 Generating Cloud Fields

Starting from 45 Landsat scenes of marine boundary layer cloud, 341 fairly realistic two-dimensional (2D; vertical and one horizontal dimension) inhomogeneous boundary layer cloud fields are created. Each cloud field is 10 km long in the horizontal direction, to match the order of magnitude of the CERES field-of-view. These are sampled from the Landsat scenes to generate the maximum variety in terms of cloud fraction (0.003 - 1.0) and mean cloud optical depth (0.2 - 48.0). The vertical variation is generated from assumptions about the cloud microphysical properties, as described in Section 2.4 of Chambers (1997). Cloud top bumpiness is imposed to match statistics from the Lidar In-Space Technology Experiment (LITE, Loeb et al., 1998) measurements of cloud top variability. This required placing 80 percent of the thickness variability in the top of the cloud, which is different from assumptions often made about inversion-capped marine boundary layer clouds. A portion of a sample cloud field is shown in Figure 1.

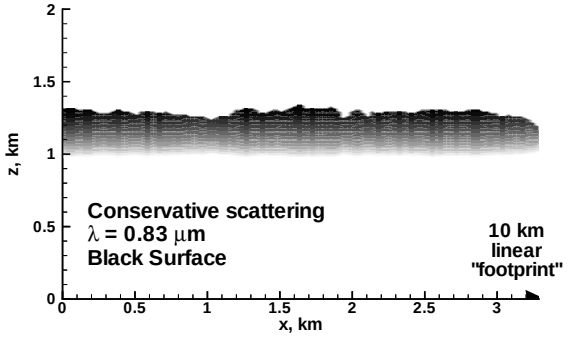

Figure 1. Portion of sample cloud field illustrates extinction variation with height in cloud and cloud-top bumpiness.

2.2 Calculating Radiance Fields

A two-dimensional radiative transfer calculation is performed using the SHDOM radiative transfer code of Evans (1998). Cyclical boundary conditions are applied. All calculations are for a 0.83 micron narrowband wavelength, and conservative scattering is assumed. The surface is black, so that only the cloud effects are considered. Radiances are calculated for 109 upwelling view angles at 10 solar zenith angles.

2.3 Building Angular Models

The computed radiances are used to build angular distribution models (ADMs) describing the angular pattern of the reflected radiation for particular types of cloud. In order to do this, a scene identification (ID), in this case cloud fraction A_c and mean cloud optical depth $\bar{\tau}_c$, is first required. This is obtained using plane parallel radiative transfer models (essentially look-up tables) applied to simulated imager data. Imager radiances are simulated from the SHDOM solution by averaging over different horizontal resolutions to simulate different imager instruments: 0.25 km simulates the high

* *Corresponding author address*: Lin H. Chambers, Atmospheric Sciences Division, Mail Stop 420, NASA Langley Research Center, Hampton, Virginia 23681-2199; e-mail <l.h.chambers@larc.nasa.gov>.

resolution images of the MODerate Resolution Imaging Spectroradiometer (MODIS) on the Terra spacecraft; 1 km simulates MODIS low-resolution images and also approximates the Visible and Infra Red Sensors (VIRS) on the TRMM spacecraft. This allows retrieval of an estimated cloud fraction and absolute optical depth.

An alternate scene ID is also assessed following Loeb et al. (1999). Rather than retrieving an absolute optical depth, this method groups scenes together in bins of fixed percentiles of radiance at each view angle, for various cloud fraction bins. This removes some view angle dependent errors.

Once a scene ID is determined, ADMs are built for each solar zenith angle as:

$$\Psi(\theta,\phi;A_c,p_t) = \pi\bar{I}(\theta,\phi)/F$$

where p_t denotes either the retrieved absolute $\bar{\tau}_c$ or the percentile bin in radiance. $\bar{I}$ is the mean radiance for all scenes corresponding to a particular scene ID at a given view and azimuth angle (θ,ϕ) and *F* is the radiance integrated over the upward hemisphere, i.e., the upwelling flux for that scene type.

2.4 Inverting Radiance to Flux

The mean ADM generated for each scene type is used to invert the radiance computed at each view angle into a retrieved flux as:

$$F_{retr}(\theta,\phi) = \pi \cdot I(\theta,\phi)/\Psi_j$$

where *j* denotes the particular scene type. The ADM used at each view angle is chosen based on the retrieved scene ID at that view angle, as would be done with radiances measured from a satellite. If there are biases in scene ID, there will also be biases in the computed flux which may have systematic behavior with view angle.

3. MODEL ASSESSMENT

To ensure that the modeling process accurately reproduces some of the actual behavior of real cloud fields, the results were first compared to features found in the literature. The model results reproduce very well the solar zenith angle bias as a function of cloud optical thickness found in Loeb and Davies (1996). They also exhibit a forward to backscatter bias in radiance identified by Loeb et al. (1998). This bias depends on the magnitude of cloud top bumpiness and results in a systematic bias in the retrieval of scene identification. The presence of these realistic features in the model results provides some confidence in the realism of the input cloud fields used, and thus in the representativeness of the flux error trends that are presented here.

4. RESULTS

4.1 Scene Identification

The scene ID is defined in this study based on cloud fraction and mean cloud optical depth (or percentile radiance interval) alone. In practical applications, additional parameters such as surface type, cloud phase, cloud height or temperature, etc, are also used. For each sample cloud field in this study, a true scene ID is known based on the extinction field that was input to SHDOM. A retrieved scene ID for the absolute $\bar{\tau}_c$ approach is calculated for different imager pixel resolutions from the pixel-averaged radiance at each direction as follows:

- a reflectance threshold is applied to the computed average simulated imager "pixel" reflectance ($R=\pi I/F$) in each direction to determine whether it is clear or cloudy
- for cloudy "pixels" a plane-parallel table look-up converts radiance at a given view and solar angle to optical depth
- results are averaged over the "pixels" in a sample cloud field to compute A_c and $\bar{\tau}_c$

For the percentile approach, the same first step is used to retrieve the cloud fraction; then scenes are grouped in fixed percentile intervals of radiance at each angle (see Loeb et al., 1999). That is for example, the brightest scenes at each angle are grouped together.

Figure 2 summarizes the errors in retrieved A_c and $\bar{\tau}_c$ for various classes of true cloudiness and for two imager resolutions. The right-hand column of results shows the errors when International Satellite Cloud Climatology Project (ISCCP; Schiffer and Rossow, 1983) rather than CERES reflectance thresholds are used. ISCCP uses a threshold which varies as the inverse cosine of solar zenith angle (Wielicki and Parker, 1992; Section 4), while the CERES threshold varies with both view and solar angles, as determined by compositing large numbers of measurements (CERES, 1995).

Note in Figure 2 that the largest cloud fraction retrieval errors occur for broken cloud fields, defined as 40 to 99 % cloudiness. Also note that for such cloud fields nadir view is not a preferred viewing direction if accurate cloud fraction is desired. Cloud fraction error for overcast cloud fields is very small, as expected. Optical depth is

generally underestimated, even for nadir view; but can be significantly overestimated from view angles in the backscatter direction.

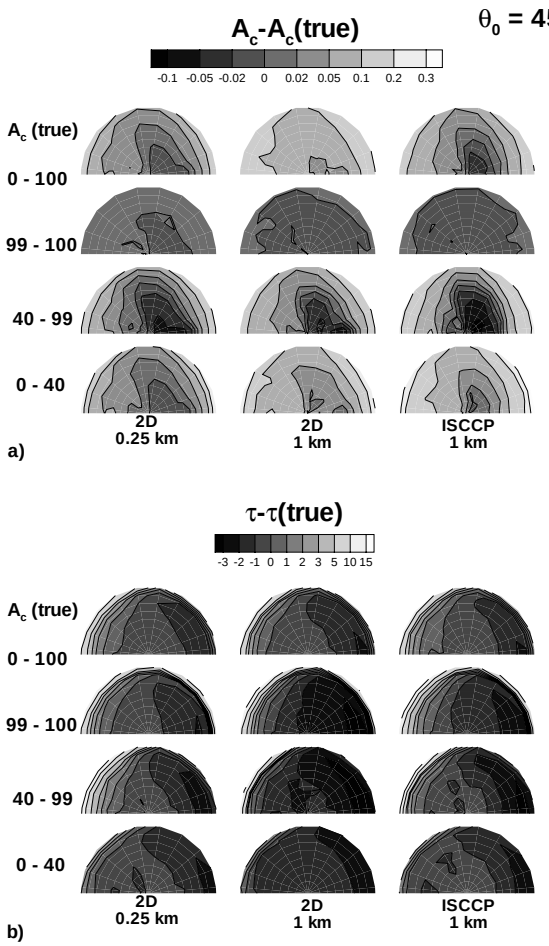

Figure 2. Scene identification error in absolute $\bar{\tau}_c$ method as a function of view angle for scattered (A_c=0-40%), broken (40-99%), overcast (99-100%), and all clouds. Solar zenith angle is 45°. Nadir view is the center of the hemisphere. Backscatter directions are on the left; forward scatter on the right.

4.2 Flux

Given a scene identification at each angle, the appropriate ADM is chosen to invert the calculated radiance to a hemispherical flux. From the SHDOM calculation, the true flux is also known. It is therefore possible to examine the error in the retrieved flux. Figure 3 summarizes the bias and root-mean-square (RMS) errors for various approaches and solar zenith angles using the absolute $\bar{\tau}_c$ scene ID. The error is averaged over all viewing angles, with the error bars denoting the variability with view angle. The 28.5 m result is for a hypothetical imager with the spatial resolution of Landsat. The two sets of results on the right-hand-side of this figure labeled "Table Look-up" are the results for fluxes calculated using a traditional plane-parallel table look-up based on A_c and $\bar{\tau}_c$. There is a substantial improvement in the flux bias error, and even in the RMS error, when the empirical ADM approach is used instead. However, even when using the ADM, the bias error estimated in this study approaches the accuracy goal limit for CERES. Further study with additional data and alternate approaches is warranted to examine this issue.

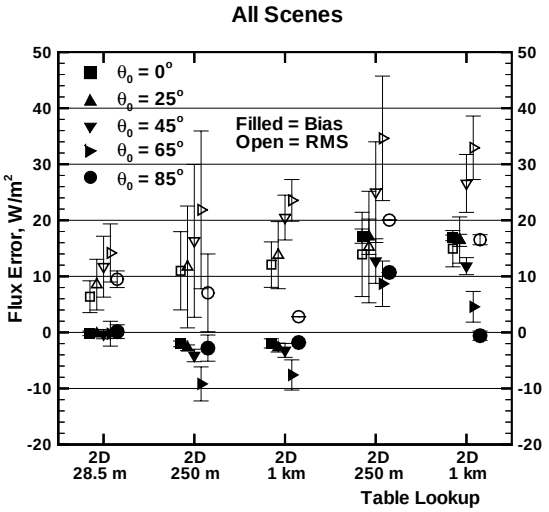

Figure 3. Summary of flux errors averaged over view angle for various imager resolutions and scene ID retrieval methods, all with absolute $\bar{\tau}_c$ scene ID. Error bars denote the variation in the error with view angle.

More interesting, perhaps, than the average error is the distribution of this error over the view angle space, which is shown in Figure 4. Due to the systematic bias in scene identification as a function of view angle, there is also a systematic variation of the flux bias in view angle space. It might be assumed that this bias will average out as more and more measurements are taken. However, attention must be given to the view angle space sampled by a particular satellite instrument to ensure that it samples evenly from the viewing hemisphere such that the bias does indeed average out. This is not necessarily guaranteed for all spacecraft/instrument combinations.

Finally, the distribution of flux error when the percentile approach is used to build the ADMs is given in Fig. 5. The maximum flux error using this method is substantially smaller than with the abo-

lute $\bar{\tau}_c$ method; and the systematic nature of the error distribution is changed.

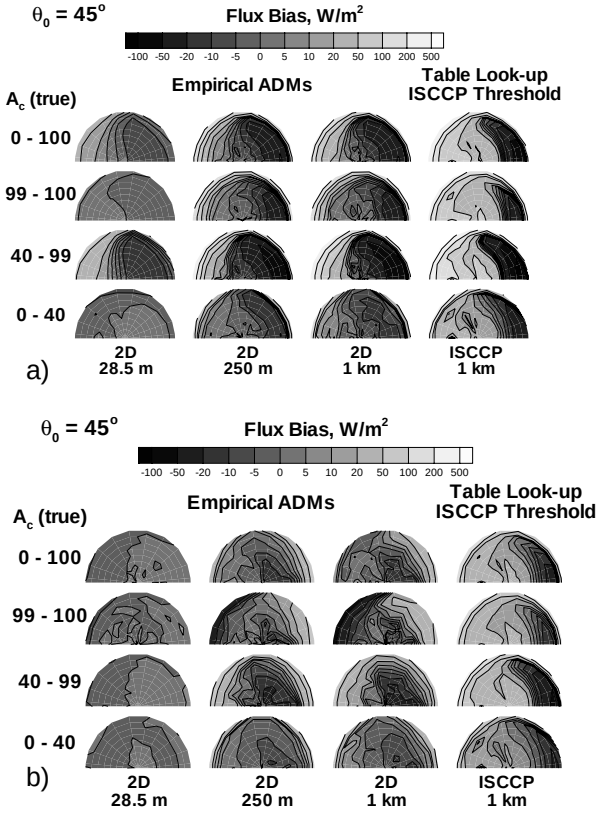

Figure 4. Distribution of flux error with view angle for different cloud fraction classes, imager resolutions, and scene ID retrieval methods. (a) with absolute $\bar{\tau}_c$ scene ID. (b) with percentile ID.

5. CONCLUSIONS AND PLANS

This paper presents a summary analysis applicable to the CERES instrument on the TRMM and Terra spacecraft, and more generally to any measurement which requires conversion of radiance to flux. It demonstrates that caution is required when using fluxes obtained from satellites which may preferentially sample one portion of the view angle space. It is shown that bias in plane parallel cloud property retrievals can be a significant source of error in estimating radiative flux. An alternate scene identification method is found to produce quite different errors and error patterns. Work is continuing to assess these two different methods and to study additional details of the retrieval algorithms in order to isolate and remove individual error sources. The results will be used to inform the uncertainty analysis for cloud property and flux retrievals, in particular those performed by CERES. Future efforts will also include additional factors such as different cloud types and the effect of varying field-of-view size, and will use additional data sources to generate improved cloud fields.

6 REFERENCES

CERES Science Team, 1995, “Clouds and the Earth’s Radiant Energy System (CERES) Algorithm Theoretical Basis Document. Vol. III-Cloud Analyses and Determination of Improved Top of Atmosphere Fluxes (Subsystem 4),” NASA RP 1376, Vol. III.

Chambers, Lin H., 1997, "Computation of the Effects of Inhomogeneous Clouds on Retrieval of Remotely Sensed Properties," Ninth Conference on Atmospheric Radiation, American Meteorological Society, Long Beach, CA.

Evans, K. Franklin, "The Spherical Harmonics Discrete Ordinate Method for Three-Dimensional Atmospheric Radiative Transfer," *J. Atmos. Sci.*, **55**, 1 February, 1998, 429-446.

Loeb, Norman G., and Roger Davies, 1996, "Observational Evidence of Plane Parallel Model Biases: The Apparent Dependence of Cloud Optical Depth on Solar Zenith Angle," *J. Geophys. Res.*, **101**, No. D1, 1621-1634.

Loeb, Norman G., Frédéric Parol, Jean-Claude Buriez and Claudine Vaubance, “Top-of-Atmosphere Albedo Estimation from Angular Distribution Models Using Scene Identification from Satellite Cloud Property Retrievals,” submitted to *J. Clim.*, March, 1999.

Loeb, Norman G., Tamas Varnai, and David M. Winker, 1998, “Influence of Subpixel-Scale Cloud-Top Structure on Reflectances from Overcast Stratiform Cloud Layers,” *J. Atmos. Sci.*, **55**, 2960-2973.

Schiffer, R. A., and W. B. Rossow, 1983, “The International Satellite Cloud Climatology Project (ISCCP): The first project of the World Climate Research Program,” *Bull. Amer. Meteor. Soc.*, **64**, 779-784.

Wielicki, B. A., and L. Parker, 1992, “On the Determination of Cloud Cover from From Satellite Sensors: The Effect of Sensor Spatial Resolution,” *J. Geophys. Res.*, **97**, No. D12, 12,799-12,823.